American Mineralogist, Volume 91, pages 907–916, 2006

Fe^{2+} and Fe^{3+} quantification by different approaches and f_{O_2} estimation for Albanian Cr-spinels

MARCO QUINTILIANI, GIOVANNI B. ANDREOZZI,* AND GIORGIO GRAZIANI

Dipartimento di Scienze della Terra, Università degli Studi di Roma "La Sapienza," Piazzale Aldo Moro 5, I-00185 Roma, Italy

ABSTRACT

Fourteen Cr-spinels from Albanian ophiolites were examined. Fe^{2+}/Fe^{3+} ratios were obtained by ^{57}Fe Mössbauer spectroscopy (MS) and compared with ratios retrieved by electron microprobe analyses (EMPA). MS spectra were collected at both 298 K (RT) and 77 K (LT), and fitted using various interpretative models. Fe^{3+} contents by EMPA, calculated from spinel stoichiometry, are almost always underestimated with respect to those obtained by MS. Moreover, Fe^{3+} contents by MS-RT are shown to be somewhat overestimated with respect to those by MS-LT, which are proved to be the most reliable. On basis of MS results, Albanian Cr-spinels proved to be non-stoichiometric, with an oxidation degree, z, ranging from 4 to 49%. Our results indicate no dependence of z on sample provenance, but suggest a strong dependence on spinel composition. Chemical data of Albanian spinel and associated olivine were used to estimate f_{O_2} via oxygen geobarometry. Notably, f_{O_2} values calculated on basis of the EMPA data are always largely underestimated with respect to those obtained on basis of MS data. However, f_{O_2} values calculated on basis of MS-RT data are equal to or higher than (up to 0.2 log units) f_{O_2} values based on MS-LT data. The increase in f_{O_2} responsible for spinel oxidation was tentatively estimated to be less than one log unit for poorly oxidized samples, but up to 6 log units for the most oxidized samples.

Keywords: Analysis, chemical (mineral), chromite, olivine, Mössbauer spectroscopy, thermobarometry, olivine-spinel

INTRODUCTION

It is generally accepted that the composition of mantle fluid phases attending magmatic and metasomatic processes strongly depends on oxygen fugacity (f_{O_2}). As an example, in the C-H-O system, the fluid phase consists mainly of CO_2 and H_2O in relatively oxidizing conditions close to the fayalite-magnetite-quartz (FMQ) solid buffer, H_2O and CH_4 in moderately oxidizing conditions between the FMQ and iron-wustite (IW) buffers, and CH_4 below IW (Wood and Virgo 1989). Several studies on mineral assemblages have been carried out to estimate mantle intensive parameters (T, P, f_{O_2}) and their evolution (e.g., Mattioli and Wood 1986; McCammon et al. 2004). There are currently two methods for the quantitative estimation of upper-mantle oxidation state: experimental, by electrochemical measurements of intrinsic oxygen fugacity (Ulmer et al. 1976; Arculus et. al. 1984), and geothermobarometry (Mattioli and Wood 1986; O'Neill and Wall 1987; Wood et al. 1990; Ballhaus et al. 1990). The latter method gives an estimate of T, P, and f_{O_2} through mineral equilibria involving phases with variable Fe^{2+}/Fe^{3+} ratios, such as garnet, clinopyroxene, Fe^{3+}-bearing chromite, and magnetite. However, small errors in Fe^{2+}/Fe^{3+} ratio quantification may produce large errors in the evaluation of mantle parameters and seriously affect petrologic interpretations (Wood and Virgo 1989; Sobolev et al. 1999).

Electron microprobe analysis (EMPA) is commonly used to investigate mineral composition, but it cannot recognize the multiple oxidation states of transition metals. As a consequence, the Fe^{2+}/Fe^{3+} ratio is usually calculated from mineral stoichiometry and charge balance, i.e., for spinels, assuming a proportion of 3 cations to 4 anions. This approach totally ignores the possibility of non-stoichiometry due to Fe^{3+} excess and cation vacancies in the lattice. In the case of non-stoichiometry, therefore, systematic errors may be very large and EMPA results turn out to be of limited value because of the wrong starting assumptions.

^{57}Fe Mössbauer spectroscopy (MS) is a very effective method for investigating the actual oxidation state of Fe in minerals and their inclusions (Wood and Virgo 1989; McCammon et al. 1998; Sobolev et al. 1999). An important and frequent application of MS to spinels is determination of highly accurate Fe^{2+}/Fe^{3+} ratios and attribution of Fe^{2+} and Fe^{3+} to the tetrahedrally and octahedrally coordinated T and M sites (e.g., Andreozzi et al. 2001; Hålenius et al. 2002 and references therein). Fe^{2+}/Fe^{3+} ratios are obtained by measuring the absorption areas of Fe^{2+} and Fe^{3+} subspectra, which are proportional to the product of the number of absorption nuclei times the recoil-free fraction (f). The f factor is determined by lattice vibrations of Fe atoms, and may suffer from temperature influence (Sawatzky et al. 1969; De Grave and Van Alboom 1991; Eeckhout and De Grave 2003). Moreover, the f factors for Fe^{2+} (f_2) and Fe^{3+} (f_3) are not equal at room temperature (RT) but, in spite of this, they are commonly assumed to be equal for a given phase. De Grave and Van Alboom (1991), on the basis of measurements of many phases of known composition, noted that the assumption of equality of f_2 and f_3 causes for spinels an error up to 30% in the Fe^{2+}/Fe^{3+} ratio measured from RT spectra, leading to overestimation of Fe^{3+}

* E-mail: gianni.andreozzi@uniroma1.it

contents. Instead, the difference between f_2 and f_3 values was found to be negligible at low temperature (LT)—i.e., at liquid nitrogen temperature (77 K) or below.

On these bases, we collected RT and LT Mössbauer spectra of Cr-bearing spinels from the Albanian eastern belt ophiolites. This work closely follows a crystal-chemical study by Bosi et al. (2004) on the same samples, in which spinel chemical and structural data were discussed in detail, and the obtained cation distribution was used as a key to understand the oxidation mechanism of Fe^{2+} into Fe^{3+} and the concomitant formation of cation vacancies in the T site. In Bosi et al. (2004), MS information was used primarily to confirm the spinel non-stoichiometry. In the present paper, both RT and LT MS data are presented and discussed, various interpretative models are compared, and the resultant Fe^{3+} contents are used to calculate the degree of oxidation of the Albanian Cr-spinels. Moreover, Fe^{3+} contents obtained by MS are compared with those calculated by charge balance from EMPA results. All such data are exploited, together with the chemical composition of olivine associated with spinels, with the aim being to obtain f_{O_2} values from olivine-spinel assemblages and to evaluate the influence of Fe^{3+} quantification on f_{O_2} estimation.

Mössbauer spectroscopy on spinels: previous studies

In the literature on spinel, fitting models associated with spinel spectra often refer to RT conditions. In spite of this, the same models have been used to fit spectra collected at various temperatures. The interpretation of spinel Mössbauer spectra has been based in some cases on completely ordered cation distributions (Osborne et al. 1981, 1984) and in others on intracrystalline cation disorder (Fatseas et al. 1976; Da Silva et al. 1980; Andreozzi et al. 2001). In particular, Figueiras and Waerenborgh (1997) proposed a simple model of two Lorentzian doublets ($1Fe^{2+} + 1Fe^{3+}$), suitable for spectra collected at RT, but too approximate for those collected at LT. Da Silva et al. (1976, 1980) analyzed natural chromites over the temperature range 50 to 300 K and suggested a three-doublet model ($1Fe^{2+} + 2Fe^{3+}$), later also adopted by Mitra et al. (1991) for RT spectra of Indian chromites. For natural Cr-bearing spinels, Wood and Virgo (1989) achieved their best results for both RT and LT spectra using a three-doublet model ($2Fe^{2+} + 1Fe^{3+}$), which was used as a reference by many authors (Bonadiman et al. 2002; Carbonin et al. 1996; Mitra et al. 1991; Chen et al. 1992). Li et al. (2002) analyzed spectra of ordered natural chromites collected at various temperatures using both a quadrupole splitting distribution and a three-doublet model ($2Fe^{2+} + 1Fe^{3+}$). To fit the LT spectra of synthetic Fe^{2+}-Fe^{3+}-bearing spinels, Hålenius et al. (2002) successfully adopted a five-doublet model ($3^{T}Fe^{2+} + 1^{M}Fe^{2+} + 1^{M}Fe^{3+}$), and their results were in excellent agreement with the cation distribution obtained by Andreozzi and Lucchesi (2002) on the same samples. Fatseas et al. (1976) adopted models with six ($5Fe^{2+} + 1Fe^{3+}$) and seven ($5Fe^{2+} + 2Fe^{3+}$) doublets for chromite spectra collected at RT and LT conditions, and recommended using different fitting procedures for different cases. Recently, on natural, disordered chromites, the best agreement between LT spectra and structural data was obtained using a six-doublet ($3^{T}Fe^{2+} + 1^{M}Fe^{2+} + 1^{T}Fe^{3+} + 1^{M}Fe^{3+}$) model (Lenaz et al. 2004).

Sample description

We analyzed fourteen Cr-spinel samples coming from ultramafic rocks of the three most important massifs belonging to the eastern belt ophiolites of Albania: Tropoja, Bulqiza, and Shebenik (Table 1). In the three massifs, chromite bodies occur both in the lower portion of layered cumulates and within the underlying mantle peridotites, always associated with a dunitic envelope (Beccaluva et al. 1998). The Tropoja Ophiolitic Massif represents the northeasternmost part of the Albanian ophiolite. Two main chromite mineralizations occur from a depth of 300 m: (1) in the mantle harzburgite-dunite and in the large dunite lenses of the transition zone; and (2) in dunites of the cumulate sequence. The Bulqiza Ultramafic Massif, located in central Albania, contains the largest number of chromite ore deposits. The chromite of Bulqiza-Bater and the other main ore deposits are located in the mid-upper part of the exposed mantle harzburgites, and are concentrated in podiform chromitites within dunitic envelopes. Chromite deposits also occur in ultramafic layered cumulates of the crustal section. The Shebenik Massif, in southern Albania, is similar to the others in its petrographic and structural features, and chromite bodies were discovered at a depth of 300 m. This massif is one of the least investigated from the viewpoint of prospecting.

Ultramafic rock samples consisted of a mineral association made up of major Cr-spinel and minor Mg-olivine, with serpentine as an alteration product. Further study of each sample using powder X-ray diffraction (XRD) analysis confirmed the presence of these phases. Olivine is deeply altered into serpentine, as revealed by the mesh texture typical of serpentinization, with only unaltered relics in the central part of each crystal. The hydrothermal process that affected olivine grains had no effect on the Cr-spinel grains, which appear unaltered, with sharp edges and homogeneous surfaces.

Experimental procedures

Thin sections of ultramafic rock were prepared for both optical inspection and microprobe analysis. Moreover, about 100 g of rock were crushed and Cr-spinels were separated from the other phases. Single crystals were handpicked under a binocular microscope to yield 18–20 mg of concentrate, cleaned in an ultrasonic bath, and thoroughly ground under acetone in an agate mortar.

Table 1. Albanian Cr-spinels and associated olivine: provenance and EMPA data

Sample	Provenance	Sequence	Spinel Fe^{3+}/Fe_{tot}	Olivine $Fe^{2+}/(Fe^{2+}+Mg)$
Tro4	Tropoja Massif	tectonite	0.14	0.032
Tro6	Tropoja Massif	cumulate	0.01	0.032
Shkm1	Shkalla, Bulqiza Massif	tectonite	0.19	0.025
Shkm3	Shkalla, Bulqiza Massif	tectonite	0.17	0.045
N2	Bulqize, Bulqiza Massif	tectonite	0.13	0.052
N4	Bulqize, Bulqiza Massif	tectonite	0.11	0.052
N7	Bulqize, Bulqiza Massif	tectonite	0.18	0.052
N10	Bulqize, Bulqiza Massif	tectonite	0.15	0.052
Thkv1	Thekna, Bulqiza Massif	tectonite	0.14	0.030
Thkv2	Thekna, Bulqiza Massif	tectonite	0.19	0.030
Ba2	Bater, Bulqiza Massif	cumulate	0.07	0.030
Ba4	Bater, Bulqiza Massif	cumulate	0.21	0.030
Shb2	Shebenik Massif	tectonite	0.17	0.046
Shb4	Shebenik Massif	cumulate	0.13	0.046

Note: For spinel, Fe^{3+} was quantified by charge balance on basis of stoichiometric formula; see Bosi et al. (2004) for additional data.

Electron microprobe analysis

Analysis of both olivine-spinel assemblages and spinel single grains was carried out using a Cameca/Camebax instrument, CNR, Padova, operating at an accelerating potential of 15 kV and a sample current of 15 nA, using WDS spectrometers. Synthetic phases [MgO, MnO, ZnS, NiO, Fe_2O_3, Al_2O_3, Cr_2O_3, $Pb_5(VO_4)_3Cl$, $Ca_2Si_2O_6$, and TiO_2] were used as standards. Raw data were reduced by PAP-type correction software provided by Cameca (Pouchou and Pichoir 1984). Each element determination was accepted after checking that the intensity of the analyzed standard before and after each measurement was within 1.00 ± 0.01. Precision for major elements was usually within 1% of the actual amount present, and that of minor elements was within about 5%. Fe^{3+} contents of Cr-spinels, calculated on the basis of charge balance and stoichiometry, and Fe^{2+} contents of associated olivine, measured on the unaltered crystal cores, are listed in Table 1. Notably, Cr-spinels from rock sections and selected single grains are homogeneous chemically. Additional chemical data of Cr-spinels were reported in Bosi et al. (2004).

^{57}Fe Mössbauer spectroscopy (MS)

Mössbauer absorbers were prepared by pressing finely ground Cr-spinel samples mixed with powdered acrylic resin (Lucite) to produce self-supporting disks. The amount used corresponded to about 2 mg Fe/cm^2 and was well below an absorber density where thickness effects influence Mössbauer results. Spectra were collected at both room (298 K) and liquid-nitrogen (77 K) temperatures, using a conventional spectrometer system operating in constant acceleration mode with a ^{57}Co source in a rhodium matrix. Low-temperature measurements were performed using a continuous cryostat filled with liquid nitrogen, temperature being controlled to within ±0.2 K. Spectral data for the velocity range –4 to 4 mm/s were recorded in a multichannel analyzer using 512 channels. After velocity calibration with the aid of high purity α-iron foil spectra, the raw data were folded in 256 channels. The spectra were fitted using the Recoil 1.04 (Lagarec and Rancourt 1998) fitting program and assuming symmetrical Lorentzian peak shapes. The best fits were evaluated by reduced χ^2, and uncertainties were calculated using the covariance matrix. Errors are estimated at about ±0.02 mm/s for isomer shift (δ), quadrupole splitting (ΔE_Q) and peak width (Γ). Errors associated with doublet areas are estimated at no less than ±3% for RT spectra, due to pronounced overlap of subspectra within the spectra, and about ±2% at LT, due to better resolution.

Interpretation of ^{57}Fe Mössbauer spectra

The RT spectra of Albanian Cr-spinels show a narrow asymmetric absorption doublet with maximum quadrupole splitting of 2 mm/s, with a complex inner part between 0 and 1 mm/s. For each sample, contributions due to Fe^{2+} doublets cover the whole spectrum, whereas absorption due to Fe^{3+} contributes to the left area between 0 and 1 mm/s (Figs. 1a and 1c).

The LT spectra are dominated by a broad asymmetric absorption doublet showing maximum quadrupole splitting up to 3 mm/s and a complex inner part between 0 and 1 mm/s. Much of the whole spectrum is due to Fe^{2+} in the tetrahedral site. According to the existing literature, the observed broad absorption may be ascribed to the next-nearest-neighbor effect, i.e., non-spherical cation distribution in the second coordination sphere of the T site (Waerenborgh et al. 1990, 1994). Moreover, the inner doublets of the spectrum may be attributed to contributions from octahedrally coordinated Fe^{2+} (Larsson et al. 1994; Hålenius et al. 2002). However, these effects do not explain the large asymmetry displayed by the spectra of the whole sample; hence, an additional absorption band due to Fe^{3+} in the area between 0 and 1 mm/s must be considered (Figs. 1b and 1d). In all cases, there is no evidence for an absorption sextet contribution in the outer part of the spectra, so that the presence of magnetic phases can be excluded.

$FeCr_2O_4$ is a normal spinel with all Cr in the M sites and Fe^{2+} completely ordered in the T sites, and this would correspond to a Mössbauer spectrum containing only a singlet. However, natural chromite samples rarely have the end-member composition. Our samples, in fact, mainly contain Mg, Fe^{2+} and Cr, but also appreciable amounts of Al and Fe^{3+}, and they underwent a complex thermal history (Bosi et al. 2004). Previous authors have proven that Fe^{2+} and Fe^{3+} occupy both the T and M sites, and this accounts for the complex spectra observed here.

Both RT and LT Mössbauer spectra of our Cr-spinels were tested with more than one interpretative model, looking for the best solution with the least number of doublets and constraints. Starting from a two-doublet model and progressively adding components, an almost satisfactory fit for all spectra, both at RT and LT, was obtained with three doublets (3d, $2Fe^{2+}$ + $1Fe^{3+}$). Refined hyperfine parameters are listed in Table 2. The quadrupole splitting of Fe^{2+} reaches its highest values with decreasing temperature, whereas that of Fe^{3+} is less influenced. The dependence of Fe^{2+} quadrupole splitting on temperature and cation-site distortion in spinels has already been treated in the literature (Osborne et al. 1984; Waerenborgh et al. 1990). In a mainly normal spinel, the number of different cation configurations around $^{T}Fe^{2+}$ increases with the degree of inversion. Doublets due to these configurations have different quadrupole splitting values (next-nearest-neighbor effect), but are not resolved at RT, as they overlap in the central portion of the absorption spectra (Waerenborgh et al. 1994). Instead, LT spectra are better resolved, due to an increase of Fe^{2+} quadrupole splitting and to a less pronounced overlap of Fe^{2+} and Fe^{3+} doublets (Fig. 1, Table 2).

For a better refinement of spectral details, more components were added to the LT spectra, and a very good, unconstrained fit was obtained with five doublets ($4Fe^{2+}$ + $1Fe^{3+}$). Moreover, comparison with cation distribution obtained by Bosi et al. (2004) suggested adding a sixth Fe^{3+} doublet to account for Fe^{3+} in the M site. This was done successfully for all samples except Tro6, for which structural data suggested attributing all Fe^{3+} to the T site. The six-doublet model (6d, $4^{T}Fe^{2+}$ + $1^{T}Fe^{3+}$ + $1^{M}Fe^{3+}$) was finally chosen because it gave the best results with least constraints (Table 3). Hyperfine parameters of LT spectra show that: tetrahedrally coordinated Fe^{2+} is characterized by δ = 1.00–1.20 mm/s and ΔE_Q from 1.09 to 3.24 (due to next-nearest-neighbor effect); octahedrally coordinated Fe^{2+} is not revealed by inspection of our spectra; tetrahedrally coordinated Fe^{3+} shows hyperfine parameters δ = 0.23–0.45 mm/s and ΔE_Q from 0.33 to 0.94 mm/s; and octahedrally coordinated Fe^{3+} shows δ = 0.39–0.52 mm/s and ΔE_Q from 0.43 to 0.90 mm/s. These latter two species are difficult to distinguish solely on the basis of Mössbauer data, but the observed trend suggests that the highest δ values should be attributed to Fe^{3+} in octahedral coordination (Fig. 2).

Quantifications of Fe^{3+} and oxidation degree of Albanian Cr-spinels

The quantities of Fe^{3+} obtained from RT spectra are equal to or higher than those obtained from LT ones. Differences become pronounced at $Fe^{3+}/Fe_{tot} > 25\%$ (Fig. 3). To account for a temperature influence on Fe^{2+} and Fe^{3+} quantification, the amounts retrieved from spectral areas in both RT and LT conditions were corrected with the f values proposed for spinels by De Grave and Van Alboom (1991): for RT conditions, $f_2 = 0.687$ and $f_3 = 0.887$; for LT conditions, $f_2 = 0.886$ and $f_3 = 0.941$. The Fe^{2+}/Fe^{3+} ratios from our RT spectra corrected with f factors increased

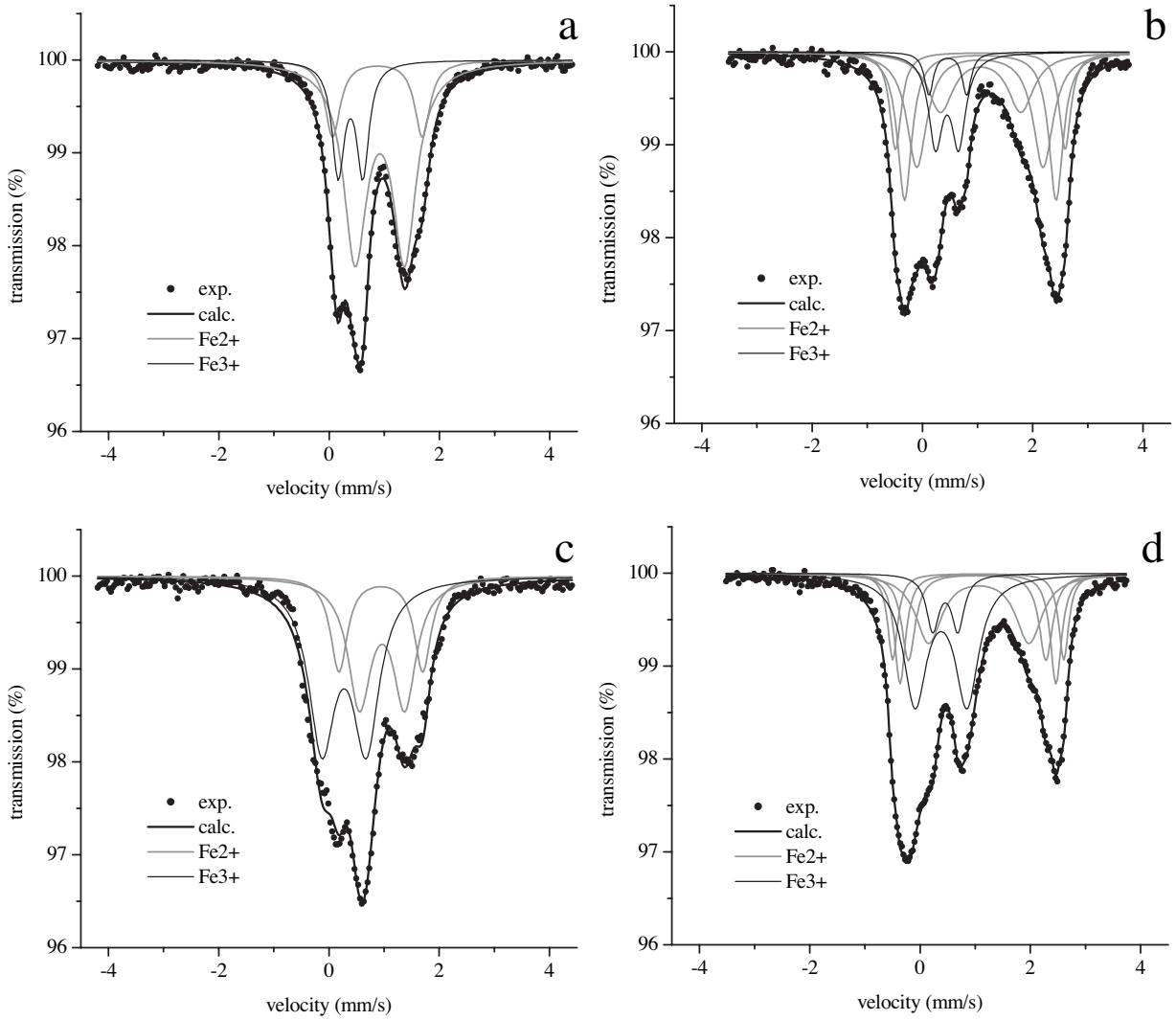

FIGURE 1. ^{57}Fe Mössbauer spectra of Albanian Cr-spinel samples Shb4 (**a, b**) and Shb2 (**c, d**) with low and high Fe^{3+} contents, respectively: spectra **a** and **c** collected at RT (fit with three-doublet model); spectra **b** and **d** collected at LT (fit with six-doublet model).

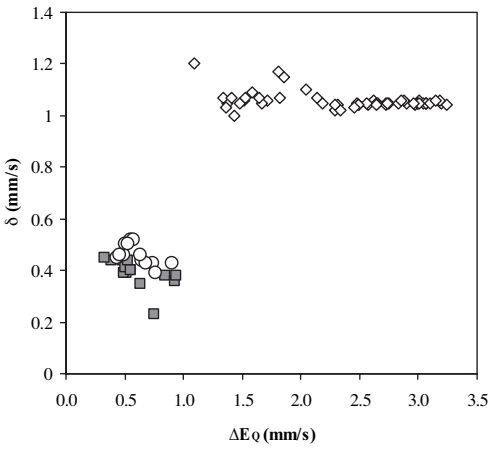

FIGURE 2. Plot of isomer shift δ (mm/s) *vs* quadrupole splitting ΔE_Q (mm/s) with evidence of Fe^{2+} and Fe^{3+} site assignment (gray squares = $^{T}Fe^{3+}$; open circles = $^{M}Fe^{3+}$; open diamonds = $^{T}Fe^{2+}$). Data from LT spectra fitted with six-doublet model (6d).

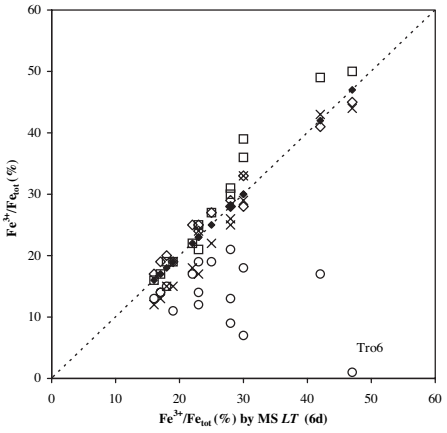

FIGURE 3. Comparison between Fe^{3+}/Fe_{tot} (%) determined by different approaches: open circles = calculated from EMPA on the basis of spinel stoichiometry; open squares = MS-RT; crosses = MS-RT corrected with *f* factors; open diamonds = MS-LT fitted with three-doublet model (3d); filled diamonds = MS-LT fitted with six-doublet model (6d). Dashed line = 1:1.

TABLE 2. ^{57}Fe Mössbauer hyperfine parameters for Albanian Cr-spinels at *RT* (298 K, left) and at *LT* (77 K, right): fit with the three-doublet model ($2Fe^{2+} + 1Fe^{3+}$)

Sample	δ (mm/s)	ΔE_Q (mm/s)	Γ (mm/s)	A (%)	δ (mm/s)	ΔE_Q (mm/s)	Γ (mm/s)	A (%)	Assignment
Tro4	0.89	1.73	0.40	30	1.05	2.90	0.42	55	Fe^{2+}
	0.92	0.97	0.50	53	1.05	2.12	0.50	26	Fe^{2+}
	0.39	0.47	0.26	17	0.47	0.47	0.36	19	Fe^{3+}
Tro6	0.95	1.47	0.34	13	1.06	2.88	0.38	26	Fe^{2+}
	0.94	0.84	0.56	37	1.17	1.93	0.56	29	Fe^{2+}
	0.29	0.79	0.60	50	0.34	0.91	0.56	45	Fe^{3+}
Shkm1	0.94	1.43	0.44	44	1.05	2.88	0.38	44	Fe^{2+}
	0.91	0.84	0.40	31	1.04	2.14	0.56	31	Fe^{2+}
	0.34	0.54	0.28	25	0.46	0.46	0.32	25	Fe^{3+}
Shkm3	0.93	1.45	0.54	43	1.05	2.91	0.36	39	Fe^{2+}
	0.94	0.81	0.44	35	1.02	2.26	0.56	36	Fe^{2+}
	0.35	0.55	0.36	22	0.47	0.51	0.40	25	Fe^{3+}
N2	0.89	1.64	0.36	20	1.05	2.08	0.42	50	Fe^{2+}
	0.92	0.90	0.50	64	1.03	2.03	0.56	33	Fe^{2+}
	0.40	0.44	0.26	16	0.49	0.44	0.34	17	Fe^{3+}
N4	0.94	1.75	0.48	43	1.04	3.03	0.32	41	Fe^{2+}
	0.90	1.08	0.52	38	1.04	2.47	0.62	40	Fe^{2+}
	0.29	0.72	0.30	19	0.45	0.63	0.40	19	Fe^{3+}
N7	0.91	1.41	0.52	33	1.06	2.90	0.34	34	Fe^{2+}
	0.95	0.74	0.46	36	1.00	2.27	0.58	38	Fe^{2+}
	0.31	0.54	0.46	31	0.46	0.53	0.40	28	Fe^{3+}
N10	0.88	1.63	0.34	17	1.05	2.81	0.44	43	Fe^{2+}
	0.92	0.90	0.50	64	1.04	2.01	0.58	37	Fe^{2+}
	0.39	0.45	0.26	19	0.47	0.45	0.38	20	Fe^{3+}
Thkv1	0.86	1.58	0.44	27	1.05	2.81	0.44	46	Fe^{2+}
	0.93	0.83	0.50	52	1.01	2.05	0.56	30	Fe^{2+}
	0.41	0.42	0.34	21	0.49	0.48	0.44	24	Fe^{3+}
Thkv2	0.91	1.41	0.52	33	1.05	2.82	0.42	41	Fe^{2+}
	0.94	0.77	0.46	40	1.01	2.09	0.58	32	Fe^{2+}
	0.34	0.49	0.36	27	0.48	0.47	0.40	27	Fe^{3+}
Ba2	0.91	1.50	0.38	17	1.05	2.80	0.44	38	Fe^{2+}
	0.97	0.77	0.48	47	0.99	2.11	0.58	29	Fe^{2+}
	0.32	0.49	0.54	36	0.48	0.51	0.48	33	Fe^{3+}
Ba4	0.90	1.49	0.46	20	1.05	2.78	0.44	46	Fe^{2+}
	0.96	0.79	0.48	50	1.00	2.00	0.70	26	Fe^{2+}
	0.35	0.47	0.42	30	0.49	0.49	0.48	28	Fe^{3+}
Shb2	0.94	1.52	0.36	18	1.05	2.89	0.36	28	Fe^{2+}
	0.96	0.82	0.50	33	1.16	1.98	0.58	31	Fe^{2+}
	0.27	0.80	0.58	49	0.33	0.95	0.52	41	Fe^{3+}
Shb4	0.92	1.47	0.50	35	1.06	2.87	0.40	38	Fe^{2+}
	0.97	0.75	0.44	34	1.01	2.23	0.58	33	Fe^{2+}
	0.32	0.49	0.50	31	0.47	0.53	0.46	29	Fe^{3+}

Notes: δ = isomer shift (with respect to α-iron); ΔE_Q = quadrupole splitting; Γ = full width at half maximum; A = area. Estimated uncertainties are about 0.02 mm/s for δ, ΔE_Q and Γ, and no less than 3% for RT spectral areas and 2% for LT spectral areas.

by about 30% with respect to those directly evaluated from the spectral areas. Consequently, using untreated RT data leads to a constant overestimation of Fe^{3+} contents, up to three–four times the experimental error. Instead, the Fe^{2+}/Fe^{3+} ratios from LT spectra corrected with *f* factors remained substantially unchanged within experimental error. This last observation highlights the advantage of collecting low-temperature data, as it yields the actual quantification of Fe^{3+} without the need of empirical correction factors.

For LT spectra, the influence of fitting models on Fe^{3+} quantification was not very large. Non-systematic effects up to 3%, which is the maximum difference between the amounts of Fe^{3+} retrieved by LT (6d) and LT (3d) spectra, were observed (Fig. 3). However, LT (6d) results allowed the assignment of Fe^{2+} and Fe^{3+} to the T and M spinel sites, achieving close agreement with the site distribution obtained from structural data (Bosi et al. 2004). On the basis of both high spectral definition and support of structural data, the absorption areas of Fe^{2+} and Fe^{3+} subspectra measured on LT spectra fitted with six doublets proved to be the most reliable due to their accuracy and precision, and were then used to quantify the actual Fe^{3+} contents.

Comparisons between spinel Fe^{3+} contents measured by MS

TABLE 3. ^{57}Fe Mössbauer hyperfine parameters for Albanian chromites at 77 K: fit with the six-doublets model (6d) and site attributions

Sample	δ (mm/s)	ΔE_Q (mm/s)	Γ (mm/s)	A (%)	Sample	δ (mm/s)	ΔE_Q (mm/s)	Γ (mm/s)	A (%)	Assignment
Tro4	1.05	3.20	0.20	9	N10	1.05	3.07	0.26	13	$^{T}Fe^{2+}$
	1.05	2.90	0.28	26		1.05	2.74	0.32	24	$^{T}Fe^{2+}$
	1.05	2.48	0.44	32		1.04	2.29	0.44	27	$^{T}Fe^{2+}$
	1.09	1.59	0.56	16		1.05	1.48	0.60	18	$^{T}Fe^{2+}$
	0.44	0.39	0.28	7		0.45	0.33	0.24	8	$^{T}Fe^{3+}$
	0.44	0.65	0.26	10		0.46	0.63	0.24	10	$^{M}Fe^{3+}$
Tro6	1.06	3.01	0.28	15	Thkv1	1.06	3.18	0.20	6	$^{T}Fe^{2+}$
	1.06	2.62	0.32	18		1.06	2.88	0.26	20	$^{T}Fe^{2+}$
	1.15	1.86	0.42	17		1.04	2.49	0.40	29	$^{T}Fe^{2+}$
	1.20	1.09	0.24	3		1.07	1.64	0.56	22	$^{T}Fe^{2+}$
	0.38	0.85	0.60	47		0.35	0.63	0.32	9	$^{T}Fe^{3+}$
	–	–	–	–		0.52	0.57	0.42	14	$^{M}Fe^{3+}$
Shkm1	1.05	3.00	0.28	25	Thkv2	1.05	3.00	0.28	19	$^{T}Fe^{2+}$
	1.05	2.65	0.32	21		1.05	2.64	0.34	23	$^{T}Fe^{2+}$
	1.07	2.14	0.42	18		1.05	2.18	0.42	19	$^{T}Fe^{2+}$
	1.05	1.38	0.56	13		1.03	1.36	0.56	14	$^{T}Fe^{2+}$
	0.23	0.75	0.20	1		0.41	0.50	0.28	8	$^{T}Fe^{3+}$
	0.46	0.49	0.28	22		0.50	0.53	0.38	17	$^{M}Fe^{3+}$
Shkm3	1.05	3.06	0.26	19	Ba2	1.05	3.01	0.28	15	$^{T}Fe^{2+}$
	1.05	2.72	0.32	23		1.04	2.64	0.34	21	$^{T}Fe^{2+}$
	1.02	2.29	0.44	23		1.10	2.04	0.48	22	$^{T}Fe^{2+}$
	1.00	1.43	0.56	13		1.07	1.34	0.56	12	$^{T}Fe^{2+}$
	0.40	0.55	0.28	9		0.36	0.93	0.44	17	$^{T}Fe^{3+}$
	0.52	0.55	0.36	13		0.45	0.43	0.30	13	$^{M}Fe^{3+}$
N2	1.05	3.06	0.24	17	Ba4	1.05	2.96	0.32	24	$^{T}Fe^{2+}$
	1.05	2.75	0.30	24		1.05	2.56	0.34	22	$^{T}Fe^{2+}$
	1.04	2.31	0.42	25		1.17	1.81	0.34	11	$^{T}Fe^{2+}$
	1.06	1.52	0.56	18		1.07	1.41	0.56	15	$^{T}Fe^{2+}$
	0.39	0.52	0.22	5		0.40	0.55	0.22	5	$^{T}Fe^{3+}$
	0.50	0.51	0.30	11		0.39	0.76	0.48	23	$^{M}Fe^{3+}$
N4	1.04	3.24	0.20	13	Shb2	1.05	3.10	0.22	10	$^{T}Fe^{2+}$
	1.04	2.97	0.26	27		1.05	2.83	0.24	13	$^{T}Fe^{2+}$
	1.04	2.57	0.38	26		1.04	2.49	0.30	21	$^{T}Fe^{2+}$
	1.06	1.71	0.56	15		1.07	1.82	0.56	14	$^{T}Fe^{2+}$
	0.39	0.49	0.30	4		0.38	0.94	0.52	34	$^{T}Fe^{3+}$
	0.43	0.74	0.32	15		0.46	0.46	0.28	8	$^{M}Fe^{3+}$
N7	1.05	3.04	0.24	19	Shb4	1.06	3.15	0.20	8	$^{T}Fe^{2+}$
	1.04	2.72	0.28	19		1.06	2.85	0.28	18	$^{T}Fe^{2+}$
	1.02	2.34	0.28	12		1.03	2.45	0.44	31	$^{T}Fe^{2+}$
	1.05	1.67	0.56	20		1.07	1.53	0.56	15	$^{T}Fe^{2+}$
	0.44	0.48	0.20	6		0.44	0.53	0.36	19	$^{T}Fe^{3+}$
	0.43	0.68	0.52	24		0.43	0.90	0.50	9	$^{M}Fe^{3+}$

Notes: δ = isomer shift (with respect to α-iron); ΔE_Q = quadrupole splitting; Γ = full width at half maximum; A = area. Estimated uncertainties are about 0.02 mm/s for δ, ΔE_Q, and Γ, and no less than 2% for spectral areas.

(Fe^{3+}_{MS}) and those calculated from EMPA on the basis of stoichiometry (Fe^{3+}_{EMPA}) revealed great differences (Fig. 3). Most Fe^{3+}_{EMPA} contents range from 7 to 21% of total Fe, with the exception of Tro6, which has 1% (Table 1). The values of Fe^{3+}_{MS} are consistently higher than Fe^{3+}_{EMPA}: the difference is very large for samples Shb4, Ba2 and Shb2 (+15, +23, and +25% of total Fe, respectively), and extremely large for Tro6 (+46% of total Fe). These differences confirmed the difficulty of microprobe analysis for accurate Fe^{3+} determination, as already observed by Wood and Virgo (1989).

A major part of the very large differences in Fe^{3+} contents observed in our samples is due to non-stoichiometry. As already mentioned, the Fe^{3+}_{EMPA} calculated by charge balance cannot reveal an Fe^{3+} excess, whereas Mössbauer results played a crucial role in revealing the Fe^{3+} excess of Albanian Cr-spinels (Bosi et al. 2004). In particular, the latter authors interpreted the Fe^{3+} excess as due to oxidation, and distinguished Fe^{2+} and Fe^{3+} of primary mineral formation (Fe^{2+}_P and Fe^{3+}_P) from Fe^{3+} derived by subsequent oxidation (Fe^{3+}_S, defined as the difference between Fe^{3+}_{MS} and Fe^{3+}_P). During the spinel oxidation process, only Fe^{2+} and Fe^{3+} changed their ratios, as the other cations were not involved. In this process, tetrahedrally coordinated Fe^{2+}_P oxidized to Fe^{3+}_S with the formation of a cation vacancy in the T site ($^{T}\square$), as described by the general oxidation mechanism:

$$2\ Fe^{2+}_P + O \rightarrow 2\ Fe^{3+}_S + O^{2-} + {}^{T}\square$$

Following Menegazzo et al. (1997), we used crystal-chemical data to calculate the degree of oxidation, z:

$$z = 8\ {}^{T}\square/(3 - {}^{T}\square)\ Fe^{2+}_P$$

The parameter z may be used to reconstruct the oxidation history of spinel samples: when $z = 0\%$ there is no evidence of oxidation (no Fe^{3+}_S formation), when $z = 100\%$ there is maximum

TABLE 4. Albanian Cr-spinels and associated olivine: chemical data obtained by different analytical approaches and corresponding f_{O_2} values (in Δlog units with respect to FMQ)

Sample	Analytical approach	Spinel				Olivine	$\Delta\log(f_{O_2})_{FMQ}$
		$X^{sp}_{(Fe2+)}$	$X^{sp}_{(Fe3+)}$	$X^{sp}_{(Al)}$	$X^{sp}_{(Cr)}$	$X^{ol}_{(Fe2+)}$	
	EMPA	0.390	0.032	0.285	0.706	0.032	+1.7
Tro4	EMPA+MS *RT*	0.381	0.038	0.283	0.706	–	+2.0
	EMPA+MS *LT* (6d)	0.381	0.038	0.283	0.706	–	+2.0
	EMPA	0.368	0.002	0.195	0.805	0.032	–3.2
Tro6	EMPA+MS *RT*	0.227	0.085	0.178	0.805	–	+3.0
	EMPA+MS *LT* (6d)	0.238	0.081	0.179	0.805	–	+2.9
	EMPA	0.314	0.037	0.220	0.771	0.025	+2.3
Shkm1	EMPA+MS *RT*	0.298	0.048	0.218	0.771	–	+2.7
	EMPA+MS *LT* (6d)	0.303	0.048	0.219	0.771	–	+2.7
	EMPA	0.347	0.035	0.227	0.764	0.045	+1.0
Shkm3	EMPA+MS *RT*	0.333	0.045	0.225	0.764	–	+1.4
	EMPA+MS *LT* (6d)	0.333	0.045	0.225	0.764	–	+1.4
	EMPA	0.349	0.026	0.195	0.800	0.052	+0.2
N2	EMPA+MS *RT*	0.341	0.032	0.194	0.800	–	+0.5
	EMPA+MS *LT* (6d)	0.341	0.032	0.194	0.800	–	+0.5
	EMPA	0.267	0.017	0.630	0.359	0.052	–0.2
N4	EMPA+MS *RT*	0.249	0.028	0.623	0.359	–	+0.6
	EMPA+MS *LT* (6d)	0.249	0.028	0.623	0.359	–	+0.6
	EMPA	0.387	0.042	0.199	0.792	0.052	+1.1
N7	EMPA+MS *RT*	0.347	0.071	0.194	0.792	–	+1.9
	EMPA+MS *LT* (6d)	0.350	0.069	0.194	0.792	–	+1.9
	EMPA	0.400	0.035	0.183	0.810	0.052	+0.8
N10	EMPA+MS *RT*	0.388	0.044	0.182	0.810	–	+1.2
	EMPA+MS *LT* (6d)	0.391	0.042	0.182	0.810	–	+1.1
	EMPA	0.362	0.029	0.188	0.806	0.030	+1.6
Thkv1	EMPA+MS *RT*	0.337	0.047	0.186	0.806	–	+2.4
	EMPA+MS *LT* (6d)	0.337	0.047	0.185	0.806	–	+2.4
	EMPA	0.325	0.038	0.189	0.803	0.030	+2.0
Thkv2	EMPA+MS *RT*	0.303	0.053	0.187	0.803	–	+2.4
	EMPA+MS *LT* (6d)	0.309	0.050	0.187	0.803	–	+2.4
	EMPA	0.300	0.011	0.172	0.826	0.030	–0.3
Ba2	EMPA+MS *RT*	0.227	0.055	0.164	0.826	–	+2.3
	EMPA+MS *LT* (6d)	0.243	0.047	0.166	0.826	–	+2.1
	EMPA	0.293	0.039	0.179	0.814	0.030	+1.9
Ba4	EMPA+MS *RT*	0.268	0.055	0.176	0.814	–	+2.5
	EMPA+MS *LT* (6d)	0.274	0.051	0.177	0.814	–	+2.3
	EMPA	0.328	0.033	0.208	0.784	0.046	+0.8
Shb2	EMPA+MS *RT*	0.231	0.091	0.196	0.784	–	+2.3
	EMPA+MS *LT* (6d)	0.255	0.079	0.199	0.784	–	+2.1
	EMPA	0.345	0.025	0.212	0.782	0.046	+0.4
Shb4	EMPA+MS *RT*	0.295	0.059	0.205	0.782	–	+1.7
	EMPA+MS *LT* (6d)	0.304	0.053	0.206	0.782	–	+1.6

Notes: For olivine: $X^{ol}_{(Fe2+)} = Fe^{2+}/(Fe^{2+} + Mg)$. For spinel: EMPA = pre-oxidation chemical composition (Fe^{2+} and Fe^{3+} contents calculated from stoichiometry); EMPA + MS *RT* = post-oxidation chemical composition (Fe^{2+} and Fe^{3+} contents measured by combining EMPA + MS *RT* data); EMPA + MS *LT* (6d) = post-oxidation chemical composition (Fe^{2+} and Fe^{3+} contents measured by combining EMPA + MS *LT* data); $X^{sp}_{(Fe2+)} = Fe^{2+}/(Fe^{2+} + Mg)$, $X^{sp}_{(Fe3+)} = Fe^{3+}/(Cr + Al + Fe^{3+})$, $X^{sp}_{(Al)} = Al/(Cr + Al + Fe^{3+})$, $X^{sp}_{(Cr)} = Cr/(Cr + Al + Fe^{3+})$; see Bosi et al. (2004) for additional data.

oxidation (all Fe^{2+}_P oxidized to Fe^{3+}_S). Moreover, at $z = 0$, the spinel composition is perfectly stoichiometric, and therefore primary Fe^{2+} and Fe^{3+} contents may be adequately represented by Fe^{2+} and Fe^{3+} obtained by EMPA (within the experimental uncertainties of this method).

The Albanian Cr-spinels show variable degrees of oxidation ranging from 4 to 49%, which were tentatively related to the provenance of the deposits (Fig. 4). The Bulqiza samples have low values (z = 4–11%), with the exception of Ba2 (z = 27%). The two samples from Shebenik have z values higher than those from Bulqiza, with large internal variations (Shb4 = 18%; Shb2 = 32%). The two samples from Tropoja have largely different z values (Tro4 = 4%; Tro6 = 49%). In general, these data do not confirm the relation between degree of oxidation and provenance. Instead, the degree of oxidation seems to depend more on primary chemical compositions. With the exception of Shb2, the samples with the lowest Fe^{2+}_P/Fe_{tot} ratios (<90%) underwent minor oxidation, whereas those with the highest Fe^{2+}_P/Fe_{tot} ratios (>90%) underwent extreme oxidation (Fig. 5).

CONSEQUENCES OF Fe^{3+} QUANTIFICATION ON f_{O_2} ESTIMATION

As already mentioned, the estimation of f_{O_2} via geothermobarometry is dependent on the quantification of Fe^{3+} contents, which play a fundamental role in the calculation of both magnetite activity and equilibrium temperatures. The general formulation of geothermobarometric models, however, is based on mineral equilibrium and does not include cation vacancy effects; therefore, the effectiveness of these models for the oxidized Albanian Cr-spinels is not guaranteed. In spite of this, f_{O_2} was tentatively calculated on basis of the three experimental data sets (EMPA, MS-RT, and MS-LT) with the aim of showing the consequences of using different analytical approaches.

For our olivine-spinel assemblages, f_{O_2} was estimated by using the oxygen geobarometer of Ballhaus et al. (1990) at P = 1.5 GPa, with equilibrium temperatures retrieved by using the geothermometer of Ballhaus et al. (1991). The values of f_{O_2} were calculated relative to the FMQ buffer (O'Neill 1987). These models find application to pyroxene-free rocks and have

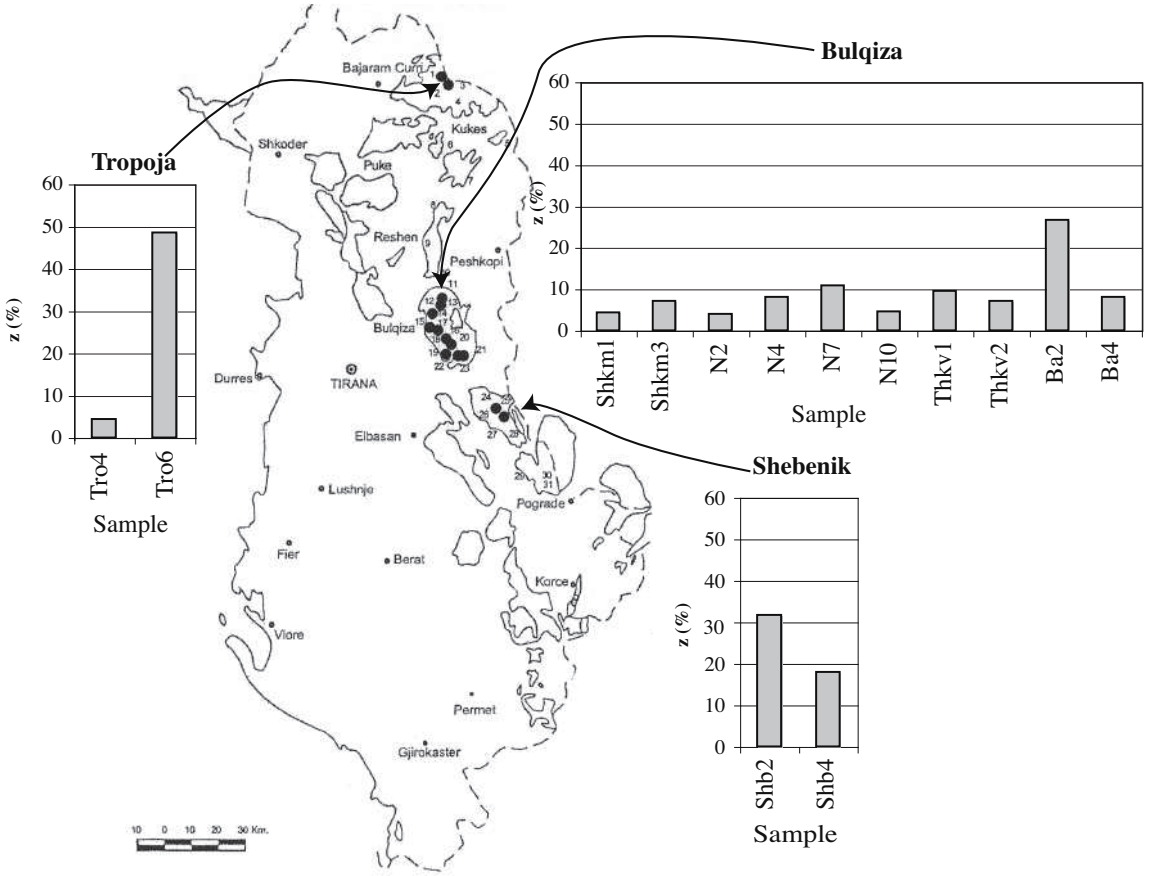

FIGURE 4. Oxidation degree z (%) of Albanian Cr-spinels as a function of the provenance of each deposit.

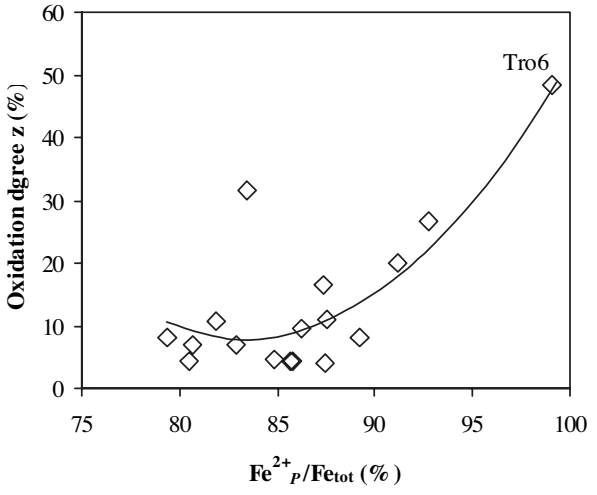

FIGURE 5. Oxidation degree z (%) as a function of Fe^{2+}_P/Fe_{tot} (%). Solid line = polynomial regression.

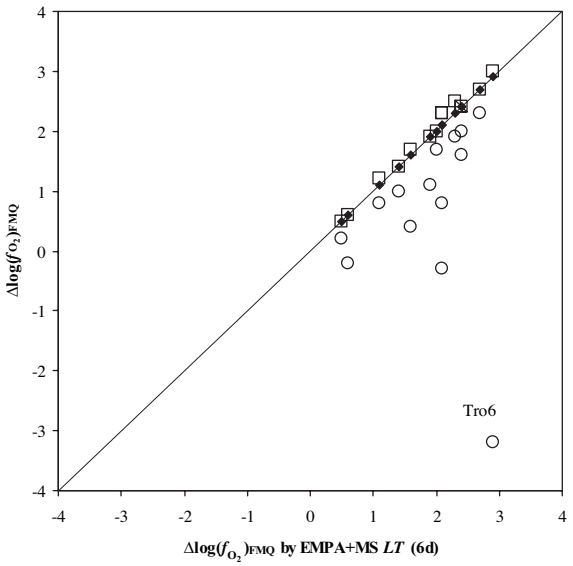

FIGURE 6. Comparison between $\Delta\log(f_{O_2})_{FMQ}$ values determined by different approaches: open circles = solely EMPA (on the basis of spinel stoichiometry); open squares = EMPA + MS-RT; filled diamonds = EMPA + MS-LT (6d). Dashed line = 1:1.

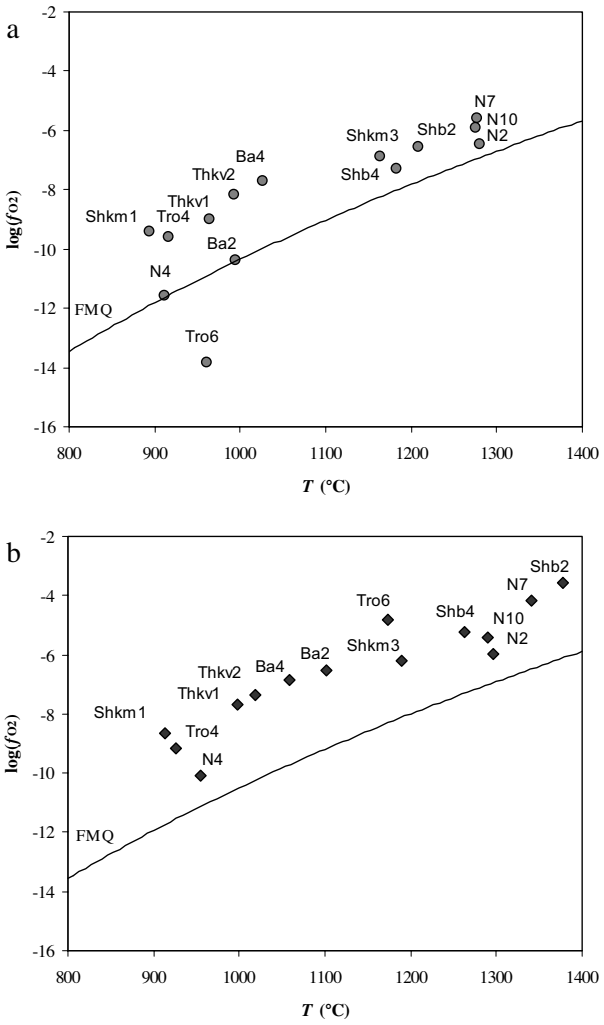

FIGURE 7. Relationship between $\log(f_{O_2})$ and equilibrium T for Albanian Cr-spinels: (**a**) pre-oxidation data; (**b**) post-oxidation data. Solid line = FMQ curve.

the advantage of working with the entire spectrum of spinel compositions (Votyakov et al. 1998). Notably, although the temperatures retrieved here are different each other and in some cases very high (and therefore should be considered with caution), the f_{O_2} values obtained here strictly depend more on Fe^{3+} contents than on T values.

Results showed that f_{O_2} values calculated solely on the basis of EMPA data are always underestimated with respect to those obtained on the basis of MS data (Fig. 6). The observed differences are in some cases very large, up to 6 log units (Table 4). Consequently, if in these cases the spinel oxidation was not taken into account, f_{O_2} values based on EMPA data would be completely misleading.

Moreover, f_{O_2} values calculated on the basis of MS-RT Fe^{3+} contents are equal to or higher than (up to 0.2 log units) f_{O_2} values calculated on basis of MS-LT data. This is a small but systematic error, which is independent of the model used.

EVALUATION OF PRE- AND POST-OXIDATION f_{O_2} VALUES

To tentatively reconstruct the Albanian Cr-spinel complex thermo-oxidative history, we need to determine their pre- and post-oxidation compositions. Pre-oxidation spinel compositions may be represented by EMPA data, because Fe^{3+} contents are calculated from spinel stoichiometry and there are no cation vacancies ($z = 0$). Instead, the present, post-oxidation spinel compositions are represented by EMPA data integrated with MS results.

Pre-oxidation $\Delta\log(f_{O_2})_{FMQ}$ values range from –3.2 to +2.3 log units, with most values close to or higher than the FMQ buffer (Fig. 7a). Post-oxidation $\Delta\log(f_{O_2})_{FMQ}$ values are systematically the highest, ranging from +0.5 to +2.9 log units (Fig. 7b). The increase in f_{O_2} responsible for spinel oxidation was estimated to be less than one log unit for poorly oxidized samples ($z \leq 11\%$), quite large (1.2–2.4 log units) for the highly oxidized samples Shb4, Ba2, and Shb2 ($18 \leq z \leq 32\%$), and extremely large (6.1 log units) for the most oxidized sample Tro6 ($z = 49\%$).

ACKNOWLEDGMENTS

F. Bosi, A.M. Conte, A. Della Giusta, S. Lucchesi, M. Lustrino, and C. Perinelli are gratefully acknowledged for stimulating discussions and suggestions, and V. Ferrini also for kindly providing the Albanian samples. G. Walton revised the English text. This work was funded by COFIN 2001 to G.G. "Evoluzione strutturale e transizioni di fase nei minerali in funzione di temperatura pressione e composizione" and was carried out within CNR-IGG research priorities. M.D. Dyar and R.F. Dymek are thanked for careful editorial handling, M. Mellini and an anonymous referee for constructive revision.

REFERENCES CITED

Andreozzi, G.B. and Lucchesi, S. (2002) Intersite distribution of Fe^{2+} and Mg in the spinel (sensu-stricto)-hercynite series by single-crystal X-ray diffraction. American Mineralogist, 87, 1113–1120.

Andreozzi, G.B., Hålenius, U., and Skogby, H. (2001) Spectroscopic active $^{IV}Fe^{3+}$-$^{VI}Fe^{3+}$ clusters in spinel-magnesioferrite solid solution crystals: a potential monitor for ordering in oxide spinels. Physics and Chemistry of Minerals, 28, 435–444.

Arculus, R.J., Dawson, J.B., Mitchell, R.H., Gust, D.A., and Holmes, R.D. (1984) Oxidation states of the upper mantle recorded by megacryst ilmenite in kimberlite and type A and B spinel lherzolites. Contributions to Mineralogy and Petrology, 85, 85–94.

Ballhaus, C., Berry, R.F., and Green, D.H. (1990) Oxygen fugacity controls in the Earth's upper mantle. Nature, 349, 437–449.

——— (1991) High pressure experimental calibration of the olivine-orthopyroxene-spinel oxygen geobarometer: implications for the oxidation state of the upper mantle. Contributions to Mineralogy and Petrology, 107, 27–40.

Beccaluva, L., Coltorti, M., Ferrini, V., Saccani, E., Siena, F., and Zeda, O. (1998) Petrological modelling of Albanian Ophiolites with particular regard to the Bulqiza chromite ore deposits. Periodico di Mineralogia, 67, 7–23.

Bonadiman, C., Ronconi, F., and Sacerdoti, M. (2002) Determinazione del rapporto Fe^{3+}/Fe^{2+} in alcune cromiti ad alto contenuto in cromo delle ofioliti dell'Albania. Plinius, 28, 67–69 (in Italian).

Bosi, F., Andreozzi, G.B., Ferrini, V., and Lucchesi, S. (2004) Behavior of cation vacancy in kenotetrahedral Cr-spinels from Albanian eastern belt ophiolites. American Mineralogist, 89, 1367–1373.

Carbonin, S., Russo, U., and Della Giusta, A. (1996) Cation distribution in some natural spinels from X-ray diffraction and Mössbauer spectroscopy. Mineralogical Magazine, 60, 335–368.

Chen, Y.L., Xu, B.F., Chen, J.G., and Ge, Y.Y. (1992) Fe^{+2}-Fe^{+3} ordered distribution in chromite spinels. Physics and Chemistry of Minerals, 19(4), 255–259.

Da Silva, E.G., Abras, A., and Sette Camara, A.O.R. (1976) Mössbauer effect study of cation distribution in natural chromites. Journal of Applied Physics, 12, 783–785.

Da Silva, E.G., Abras, A., and Speziali, L. (1980) Mössbauer effect study of cation distribution in natural chromites of Brazilian and Philippine origin. Journal of Applied Physics, 12, 389–392.

De Grave, E. and Van Alboom, A. (1991) Evaluation of ferrous and ferric Mössbauer fraction. Physics and Chemistry of Minerals, 18, 337–342.

Eeckhout, S.G. and De Grave, E. (2003) Evaluation of ferrous and ferric Mössbauer

fraction. Part II. Physics and Chemistry of Minerals, 30, 142–146.
Fatseas, G.A., Dormann, J.L., and Blanchard, H. (1976) Study of the Fe^{3+}/Fe^{2+} ratio in natural chromites $(Fe_xMg_{1-x})(Cr_{1-y-z}Fe_yAl_z)O_4$. Journal of Physics, 12, 787–792.
Figueiras, J. and Waerenborgh, J.C. (1997) Fully oxidized chromite in the Serra Alta (South Portugal) quartzites: chemical and structural characterization and geological implications. Mineralogical Magazine, 61, 627–638.
Hålenius, U., Skogby, H., and Andreozzi, G.B. (2002) Influence of cation distribution on the optical absorption spectra of Fe^{3+}-bearing spinel s.s.-hercynite crystals: evidence for electron transition in $^{VI}Fe^{2+}$-$^{VI}Fe^{3+}$ clusters. Physics and Chemistry of Minerals, 29, 319–330.
Lagarec, K. and Rancourt, D.G. (1998) RECOIL. Mössbauer spectral analysis software for Windows, version 1.0. Department of Physics, University of Ottawa, Canada.
Larsson, L., O'Neill, H.St.C., and Annersten, H. (1994). Crystal chemistry of synthetic hercynite ($FeAl_2O_4$) from XRD structural refinements and Mössbauer spectroscopy. European Journal of Mineralogy, 6, 39–51.
Lenaz, D., Andreozzi, G.B., Mitra, S., Bidyananda, M., and Princivalle, F. (2004) Crystal chemical and ^{57}Fe Moossbauer study of chromite from the Nuggihalli schist belt (India). Mineralogy and Petrology, 80, 45–57.
Li, Z, Ping, J.Y., Jin, M.Z., and Liu, M.L. (2002) Distribution of Fe^{2+} and Fe^{3+} and next-nearest neighbor effects in natural chromites: comparison between results of QSD and Lorentian doublet analysis. Physics and Chemistry of Minerals, 29, 485–494.
Mattioli, G.S. and Wood, B.J. (1986) Upper mantle oxygen fugacity recorded by spinel lherzolites. Nature, 322, 626–628.
McCammon, C.A., Chinn, I.L., Gurney, J.J., and McCallum, M.E. (1998) Ferric iron content of mineral inclusions in diamonds from George Creek, Colorado determined using Mössbauer spectroscopy. Contributions to Mineralogy and Petrology, 133, 30–37.
McCammon, C.A., Lauterbach, S., Seifert, F., Langenhorst, F., and Van Aken, P.A. (2004) Iron oxidation state in lower mantle mineral assemblages I. Empirical relations derived from high-pressure experiments. Earth and Planetary Science Letters, 222, 435–449.
Menegazzo, G., Carbonin, S., and Della Giusta, A. (1997) Cation vacancy distribution in an artificially oxidized natural spinel. Mineralogical Magazine, 61, 411–421.
Mitra, S., Pal, T., and Pal, T. (1991) Petrogenetic implication of the Mössbauer hyperfine parameters of Fe^{3+}-chromites from Sukinda (India) ultramafites. Mineralogical Magazine, 55(4), 535–542.
O'Neill, H.St.C. (1987) The quartz-fayalite-iron and quartz-fayalite-magnetite equilibria and free energies of formation of fayalite (Fe_2SiO_4) and magnetite (Fe_3O_4). American Mineralogist, 72, 67–75.
O'Neill, H.St.C. and Wall, V.J. (1987) The olivine-orthopiroxene-spinel oxygen geobarometer, the nickel precipitation curve, and the oxygen fugacity of the Earth upper mantle. Journal of Petrology, 28, 1169–1191.
Osborne, M.D., Fleet, M.E., and Bancroft, G.M. (1981) Fe^{+2}-Fe^{+3} ordering in chromite and Cr-bearing spinels. Contributions to Mineralogy and Petrology, 77, 251–255.
——— (1984) Next-nearest neighbor effects in the Mössbauer spectra of (Cr,Al) spinels. Journal of Solid State Chemistry, 53, 174–183.
Pouchou, J.L. and Pichoir, F. (1984) A new model for quantitative X-ray microanalysis. I. Application to the analysis of homogeneous samples. La Recherche Aérospatiale, 3, 13–36.
Sawatzky, G.A., Van Der Woude, F., and Morrish, A.H. (1969) Recoilness-fraction ratio for ^{57}Fe in octahedral and tetrahedral sites of a spinel and a garnet. Physical Reviews, 183(2), 383–386.
Sobolev, V.N., McCammon, C.A., Taylor, L.A., Snyder, G.A., and Sobolev, N.V. (1999) Precise Mössbauer milliprobe determination of ferric iron in rock-forming minerals and limitations of electron microprobe analysis. American Mineralogist, 84, 78–85.
Ulmer, G.C., Rosenhauer, M., Woermann, E., Ginder, J., Drory-Wolff, A., and Wasilewski, P. (1976) Applicability of electrochemical oxygen fugacity measurements to geothermometry. American Mineralogist, 61, 661–670.
Votyakov, S.L., Chashchukhin, I.S., Uimin, S.G., and Bykov, V.N. (1998) Oxygen thermometry and barometry of chromite-bearing ultramafic rocks, examples from the South Urals: I. Mössbauer Spectroscopy of chrome spinels and the problems of olivine-spinel thermometry. Geochemistry International, 36, 706–716.
Waerenborgh, J.C., Annersten, H., Ericsson, T., Figueiredo, M.O., and Cabral, J.M.P. (1990) A Mössbauer study of natural gahnite spinels showing strongly temperature dependent quadrupole splitting distributions. European Journal of Mineralogy, 2, 267–271.
Waerenborgh, J.C., Figueiredo, M.O., and Cabral, J.M.P., and Pereira, L.C.J. (1994) Powder XRD structure refinements and ^{57}Fe Mössbauer effect study of synthetic $Zn_{1-x}Fe_xAl_2O_4$ ($0<x\leq1$) spinels annealed at different temperatures. Physics and Chemistry of Minerals, 21(7), 460–468.
Wood, B.J. and Virgo, D. (1989) Upper mantle oxidation state: Ferric iron contents of lherzolite spinels by ^{57}Fe Mössbauer spectroscopy and resultant oxygen fugacities. Geochimica et Cosmochimica Acta, 53, 1277–1291.
Wood, B.J., Bryndzia, L.T., and Johnson, K.E. (1990) Mantle oxidation state and its relationship to tectonic environment and fluid speciation. Science, 248, 337–345.

MANUSCRIPT RECEIVED JUNE 7, 2005
MANUSCRIPT ACCEPTED NOVEMBER 7, 2005
MANUSCRIPT HANDLED BY ROBERT F. DYMEK